University of California, San Diego UCSD-ENG-104

Aerosol Diagnostics for Liquid-Protected IFE Chambers

A. C. Gaeris, B. Harilal, K. Sequoia and M. S. Tillack

October 1, 2003

Fusion Division
Center for Energy Research

University of California, San Diego
La Jolla, CA 92093-0417

ABSTRACT

In this report, we survey several modern techniques for measuring the size, number density and velocity distribution of aerosol and particulates. The relevance and practicality of these techniques are assessed for application to IFE-relevant ablation plumes. Although many techniques have been developed and several vendors currently sell off-the-shelf equipment, several aspects of IFE aerosols lead to difficulty in fielding these standard tools. These unique features include very rapid (sub-microsecond) time scale, small (sub-micron) particle sizes, and the lack of *a priori* knowledge of the particle size distribution. Recommendations are provided on diagnostic techniques, which offer the best hope for affordable and effective diagnosis of IFE-relevant ablation plumes.

1. INTRODUCTION

1.1 Motivation

In liquid-protected IFE chambers, the creation of aerosol is a fundamental concern, because residual species in the chamber can interfere with driver beam propagation and target injection. Two primary mechanisms for aerosol production include:

(1) nucleation and growth in the vapor phase, and

(2) ejection from the surface, most likely due to explosive phase change.[1]

In order to study the creation, evolution and transport of aerosols in IFE chambers, suitable diagnostics are needed. The parameters that we seek to measure include particle size, number density and velocity distributions as a function of time and space.

Many techniques are available for the measurement of particle size, density and/or velocity. In fact, numerous diagnostics are commercially available. [2, 3] However these diagnostics and techniques are often limited in one way or another, and may not be suitable for the study of aerosol generation and transport in short-pulse ablation plumes.

One of the most challenging aspects of aerosol behavior in ablation plumes is the short time scale for production and transport. The time scale for x-ray and ion energy deposition in IFE chambers ranges from nanoseconds to microseconds. Similarly, the formation of aerosol takes place rather quickly. Explosive ejection occurs within 10–50 ns following the energy impulse. Based on our earlier work on homogeneous nucleation, condensation processes also may take place on a time scale less than 1 μs [4]. Therefore, nanosecond time-resolved diagnostics are highly desirable in order to provide direct observations of the production and evolution of aerosol.

Another challenging aspect of aerosol diagnosis is the small size distribution. Homogeneously condensed aerosol is expected to contain a size distribution from several nanometers up to several hundred nanometers. Explosive ejecta is expected to occur in the range of 100-500 nm. Many commercial in-situ aerosol diagnostics, such as those based on Doppler anemometry, are restricted to larger sizes (as well as slower processes). For **any** light scattering diagnostic, the signal strength is a very strong function of particle size, such that measurements below 100 nm are exceptionally challenging. In cases with a distribution containing both large and small sizes, the light scattered from smaller size particles will be difficult to resolve from light scattered by the larger ones.

Finally, the lack of *a priori* knowledge of the aerosol size distribution in ablation plumes restricts the measurement technique. Many of the more sophisticated modern scattering diagnostics require a significant amount of analysis in order to infer the particle characteristics. This analysis becomes intractable or loses accuracy if the distribution of sizes is unknown.

Table 1 summarizes the general categories of diagnostic techniques we considered. The vast majority of techniques are optical in nature, relying on the attenuation, scattering, or emission of light from the particles. A single diagnostic may not be capable of providing a complete description of the aerosol, so we have considered the possibility of multiple diagnostics, each of which provides partial information. In the following sections, we discuss each of these techniques, including their main features, key limitations and potential for application to the study of IFE-relevant ablation plumes.

TABLE 1- TYPES OF DIAGNOSTICS CONSIDERED

Particle collection on witness plates and post-test microscopic examination.
Entrainment of particles by gas into an in-line particle analyzer.
Light scattering from a witness plate or the ablation target.
Light extinction.
Laser Induced Incandescence.
Mie (elastic) Light Scattering from the plume.
Laser- and Phase-Doppler anemometry.
Laser Diffraction.
Digital Holography.

1.2 Required measurement parameter ranges

Several specific constraints to the determination of the particulates parameters—velocity, size, and concentration—originate when they are embedded in a fast and hot plasma flow.

- *Plasma expansion speeds up to 20,000 m/s.*

In previous experiments with laser-heated materials, the measured expansion speeds of plasma plumes was found to be in the order of 1,000 m/s close to the laser-heated target surface, and accelerating up to 20,000 m/s at the visible tip. Therefore, when doing a point measurement, any region inside the plasma plume sampled by the probe beam will translate forward very rapidly outside of the optically observable volume.

- *Local sample volumes* $< 10^{-21}$ m^3.

The smaller size of the sample region is approximately in the order of the cube of the tight probe beam focus diameter—the diffraction-limited Gaussian beam waist, usually in the 20-50 nm range for the usual optical focal lengths and laser wavelengths in the visible spectrum.

- *Fast measurements with temporal resolution ~1 ns.*

An optical measurement must be taken faster than the time it takes to the physical processes inside the plasma plume/particulates sampled region to evolve, or to the sampling region to move out of the detectors line of sight/collection solid angle. For example, a sample region 50 nm wide will move out of detector sight in 10 ns when moving at 5,000 m/s.

- *Plume expansion time ~10-1000 μs.*

Previous experiments have shown that the expanding plume dilutes beyond detectability or mixes with the surrounding gas at times no longer than around 1000 μs.

- *Plume lengths up to 50 mm.*

Correspondingly, these experiments have found that the unhindered longitudinal expansion of a laser-heated plasma plume goes as far as ~50 mm, before diluting beyond the range of optical detection.

- *Particle sizes—1 nm to 10 μm.*

The variation of particulate sizes immersed in the plasma plume covers several orders of magnitude, so making the measurement of individual sizes and distribution of concentration really hard, particularly for particles sized smaller than the wavelength of the laser probe beam.

As it will be seen below, most of the considered optical effects are modeled using equations that are strongly dependent on power series of the ratio of particle size D to laser probe wavelength, D/λ_{pr}. Usually the particles larger than the probe wavelength generate the largest optical signatures, hence masking the presence of the more plentiful but smaller, subwavelength size particulates.

Most of the techniques for particle size and distribution measurement require the user to assume a foreknowledged particle size distribution function. Then the constants associated to this distribution can be obtained via numerical regression of the measurements by looking for the best data fit. Examples of commonly used particulate distribution formulas can be found in Appendix 3.

- *Surrounding plasma/gas index of refraction is close to 1 at experimental pressures.*

Both the Gladstone-Dale equation for a neutral gas and the Appleton-Hartree equation for a magnetized plasma (see Appendix D) state that the index of refraction for a gas or plasma is of the form

$$n = 1 \pm f(\lambda, \rho, T, B, n_e),$$

being the second term $f(\lambda,\rho,T,B,n_e)$ of order –3 to -4 for the pressures observed during laser-heated plasma experiments. This point is further developed in Appendix D.

- *Hot surrounding plasma/gas—electron temperature 1 to 100 eV.*

The plasma is almost fully ionized close to the surface, at the higher range of temperatures, and with strong atomic light emission.

2. MEASUREMENT TECHNIQUES

This section describes several techniques, both mechanical and optical for the measurement of the parameters of particulate matter immersed in plasma flows. It is not a comprehensive list of all methods usually employed for particle sizing and flow velocimetry (see ref [5]), but only of those deemed feasible for our purposes.

2.1 Mechanical Sampling

When using mechanical sampling, a small quantity of the ejecta dispersed in the plasma flow is collected or extracted for further size, shape and concentration analysis and examination outside of

the flow. Imaging, either microscopy or field, can be used to determinate particle sizes and distributions. Optical counting and sizing by signal occultation can be also utilized.

2.1.1 Collection on Witness Plate with Off-line Analysis

The composition and distribution of the condensed droplets in the ablated ejecta can be analyzed from the material deposited on a Witness Plate, for later scrutiny using optical or electron microscopy outside the experimentation chamber.

The witness plate is usually a smooth plane surface of high quality, like a microscopy slide or optical flat, placed partially or totally intercepting the path of the ejected material.

The ejecta collected this way can be the result of single, isolated shots, separated by synchronizing the motion of the witness plate behind a masking slit with the shot frequency of the pump laser. When leaving the witness plate static, the ejecta of all of them accumulate on the same spot, after several laser pump shots. The plate is the extracted for further measurement off-line of the collected material.

The size of the droplets can be estimated from the grain size appearing on microphotographs of the plate taken later (see Figure 1). Concentration is calculated from counting the number of particles of the same size lying on a fixed specific region of the plate.

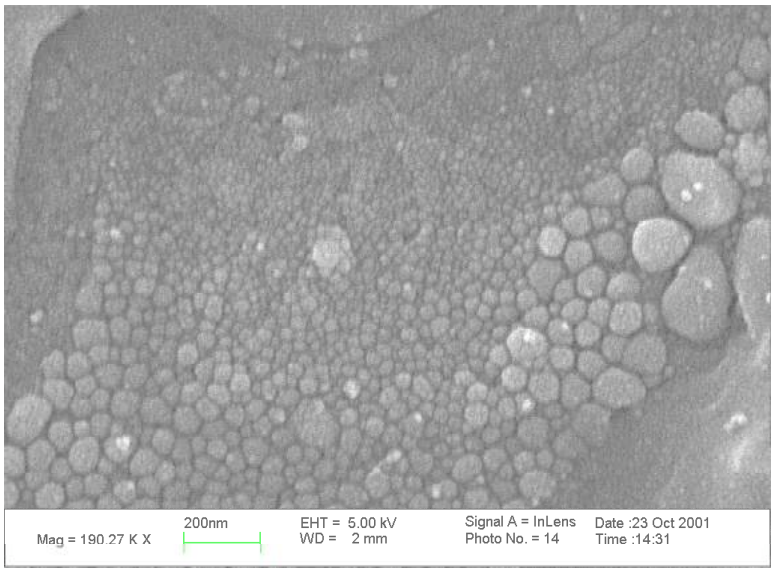

Figure 1- Electron microphotograph of the surface of a Witness Plate after the collection of ejecta from a Silicon plasma plume.

2.1.2 Gas Entraining in Off-line Analyzer

There are a few reports on in situ measurements of the size distribution of generated particles during laser ablation of solid materials. Commercially available particle sizing instruments such as Differential Mobility Analyzer (DMA), Optical Particle Counter (OPC) have been used for these

measurements. Russo and coworkers [6] measured particle size distribution of glass samples using an OPC in different laser ablation conditions.

Whitlock and Frick [7] reported that real time measurements of particle size using a DMA offer significant advantages in speed and range for studies of particulates produced by laser ablation. Typically, the target is laser ablated in a vacuum chamber, generating particles of various sizes. These particles are entrained into a carrier gas flowing through the chamber and transported into a Particle Counter or DMA (see Figure 2). The carrier gas flow rate can be adjusted for isokinetic sampling. Particle size distributions with components as small as 1 nm can be measured using DMA or OPC.

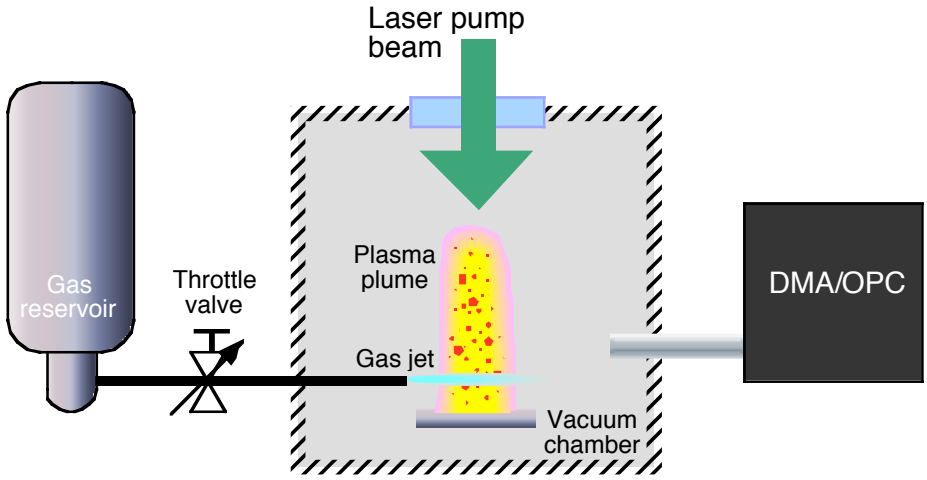

Figure 2- Layout of a Gas Entraining in Off-line Analyzer set-up.

2.1.3 Aerosol Time of Flight Mass Spectrometry

Aerosol Time of flight Mass Spectrometry (ATOFMS) has the ability to precisely determine particle size and composition in real time. A number of real time single particle mass spectrometry techniques have been described in a recent review [8].

In the ATOFMS method, particles are introduced through a nozzle, accelerated through the inlet vacuum of a mass spectrometer, attaining a terminal velocity depending upon their aerodynamic parameters. Particles encounter two intercepting continuous wave lasers which are used in conjunction with a timing circuit. The scattered signal is detected by nearby photodiodes. The time lag between the light scatter pulses can be used to calculate the velocity and diameter of single particles. Calibration curves are generated with commercially available particles of known size.

Figure 3- Block schematic for Aerosol Time of Flight Mass Spectrometry.

A schematic of the ATOFMS illustrating the main parts is shown above. The particles are introduced through a differentially pumped nozzle/skimmer arrangement. Along this passage the particles pass through the second section which is the particle sizing region where the particles encounter the laser beams oriented at right angles. In the last section, particles are vaporized and ionized by a pulsed laser. Ions produced from each particle are mass analyzed and the chemical composition is thus determined.

Unlike light scattering techniques used for particle sizing, the ATOFMS does not depend upon the particle trajectory through the laser beams.

2.1.4 Dark-Field Imaging/Scattering on Witness Plate

In this technique, the witness plate is placed in the same way that has been described in Section 2.1.1, but now the plate is probed every shot by a collimated short pulse laser beam (of different wavelength than that the pump laser). A transmissive Dark Field Imaging (DFI)† optical system takes the light scattered by the particles lying on the transparent, non-dispersive witness plate [9, 10] and image it on a gated CCD/CMOS camera (see a transmissive optical setup for forward scattering in figure 4.) A condenser lens focuses the non-scattered, still collimated laser probe light into a stop/beam dump. The light scattered by the collected ejecta particles is collimated by this lens—the focal plane of the condenser lens coincides with the surface of the witness plate. Then an imaging lens focuses it in the CCD/CMOS camera, after passing through a vignetting slit and a narrow passband interference filter (to eliminate the glare from other light sources) set for the probe laser wavelength.

The resulting image shows a dispersed field of bright dots on a dark background (as seen in Figure 5, taken using a reflective DFI setup). These dots have a brightness (calculable using Mie elastic forward-scattering theory) that is proportional to the size of the scattering particle, even for particles of diameter smaller than the probe laser wavelength.

If the witness plate is left static the accumulation of successive shots can be observed. Similarly to the standard witness plate, moving the witness plate synchronous to every pump laser shot allows to detect the discriminate the ejecta from shot to shot. An additional advantage is that the witness plate can be removed for further later examination by other methods—i.e. microscopy.

2.2 Online Optical Techniques

The classical interaction of light with solids and fluids provides several ways of ascertaining the properties of the particulate material through the changes on the parameters of the exiting light compared with the incident light, without disturbing the thermal and mechanical parameters of both the gas/plasma flow and the dispersed particulates in it.

Because they are unobtrusive to the propagation of both fluids and particles flow, several online optical methods have been developed for this purpose, usually tailored to the particular needs of the field of application. Changes in intensity, phase, frequency/wavelength, polarization, and even spatial and temporal coherence of the incident light beam, originated by *classical optical* phenomena as refraction, interference or diffraction can be measured.

---

† A reflective DFI system uses a high quality reflecting surface instead, so the optical path is now folded. See Appendix A-3 and Figure 24 for an example of a reflective DFI set-up.

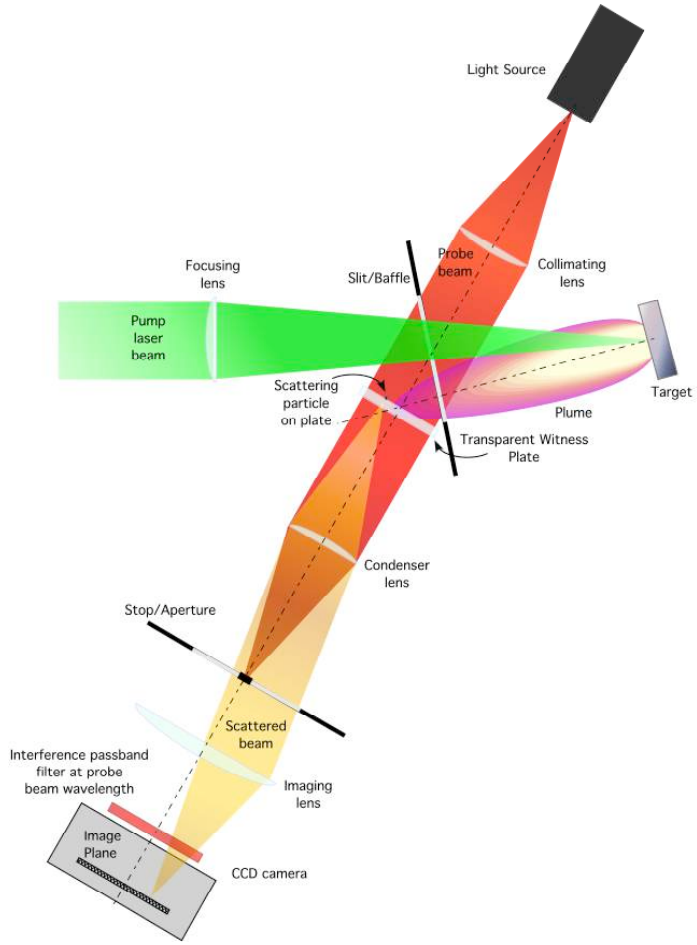

Figure 4- Optical layout for Transmissive Dark-Field Imaging of scattered light from particulates deposited on a witness plate.

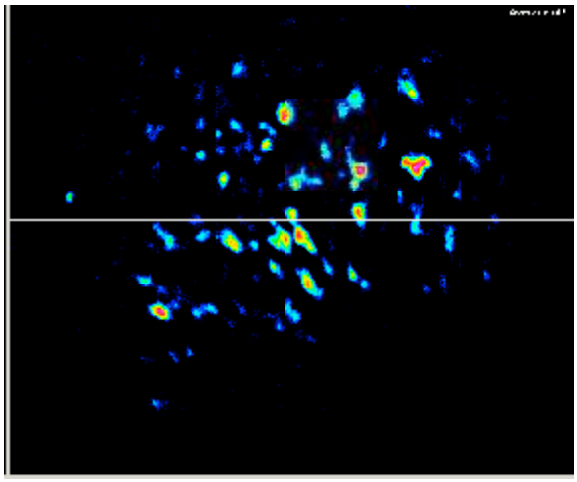

Figure 5- Reflective Dark field image of scattered He-Ne laser light from dust particles on a metallic aluminum surface. The area observed is approximately 1mm^2.

Use of fast acquisition electronics allows obtaining the temporal evolution of these parameters-'histories'-for specific, small-'single-point'-regions of the flow, or integrated global images-'snapshots'-of the full plasma plume, for each and every one laser pump shot.

Unfortunately, most of the online optical methods for particulate measurement are 'model-dependent', i.e., the final quantitative results not only depend on the quality of the observed data but also on the refinement of model that describes the light-matter interaction, plus educated guesses on particle shape and size distribution. This fact compels to the development of concurrent alternative measurement methods allowing the simultaneous validation, cross-correlation and checking of the at least some of the required parameters.

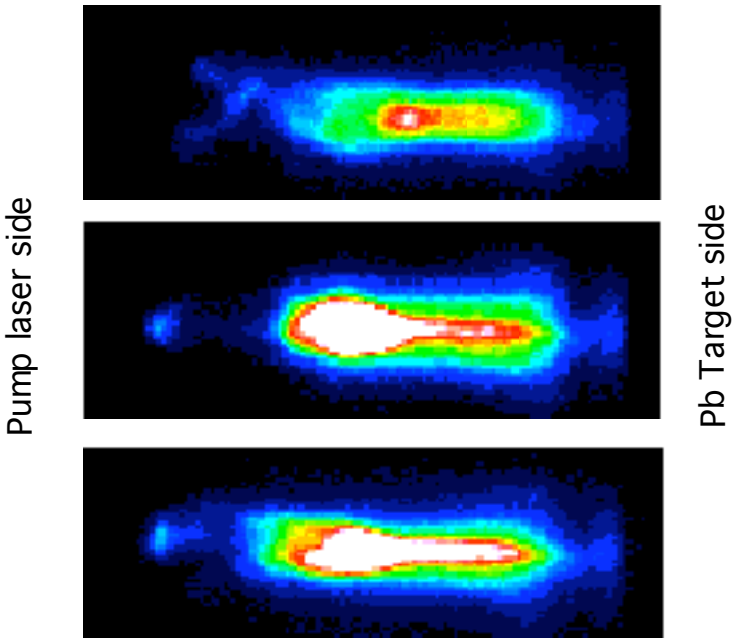

Figure 6- Lateral images of the plasma plume expansion for a Lead (Pb) target. The target is heated by a pump laser beam 7.6 ns wide and of intensity $1.1 \cdot 10^9$ W/cm^2. The plume is surrounded by a Nitrogen atmosphere at 30 Torr.

In the following sections, several common online optical methods to measure particulate size, velocity and concentration will be explained and evaluated. Some of them will include ad-hoc modifications to make them more suitable or useful to our purposes.

Table 2 shows a short list of potential online optical diagnostics for aerosols, the main measurable particle property, type of temporal response, and constraints. Other optical methods of lesser relevance or ancillary in nature are briefly descripted in Appendix A.

To simplify the experimental set-up design, plus the data acquisition and analytical procedures several assumptions on the geometry and physical parameters related to the plasma plume are made. Although only performing several 'proof of concept' experiments would verify their soundness, they will be considered valid hereon in the subsequent analysis of online optical diagnostics.

- *There are not multiple interactions of the probe beam with the particles.*

To avoid to optical attenuation/dispersion effects due to multiple particle interaction and also by limitations in the response of the electronic instrumentation for signal acquisition/processing, these techniques generally can only be applied to flows in which the dispersed particulates are in low concentration.

- *The plasma surrounding the particles must be **optically thin**, therefore:*

$$n_{ele} < \frac{m_e c^2}{4\pi e^2 \lambda_L^2} = \frac{2.824 \cdot 10^{19}}{\lambda_{Lpr[\mu m]}^2}. \qquad (1)$$

As we are dealing only with optical measurement methods, this condition guarantees that the probe beam—of wavelength λ_{Lpr}—can penetrate into the plasma plume and exit to the photodetector(s).

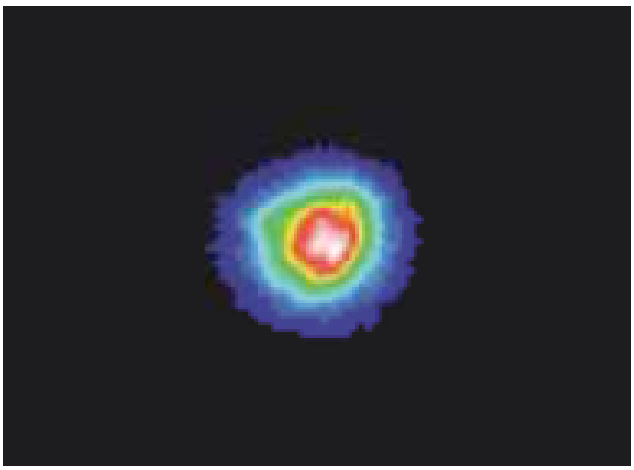

Figure 7- Front view of an expanding plasma plume.

- *Both the plasma plume density and the particle size concentration are assumed to be radially symmetric along the direction of expansion.*

These plasma plumes are formed by pump laser beams that are if not Gaussian, at least rotationally symmetric in cross-section, when heating a uniform, smooth plane material surface at normal incidence. Therefore, no reason is expected for these plumes to diverge out of the circular shape during their longitudinal expansion, even when there is a simultaneous substantial lateral expansion (see Figure 6 for lateral views and Figure 7 for a frontal view of laser-heated expansion plumes).

- *All the particles must be always spherical in shape.*

For particulates moving immersed in a plasma plume is expected that superficial tension during the liquid formation phase will produce particles that differ little from the spherical shape. This assumption is very helpful to simplify the calculations when modeling elastic light scattering (Mie) in particles.

TABLE 2- PARTICULATES/PLASMA PARAMETERS AND OPTICAL MEASUREMENT TECHNIQUES

Particle property	Method	H	S	M	R
Size	Light Extinction*	√			
	Mie Laser Scattering	√	√	√	√
	Laser Doppler Anemometry†	√		‡	
	Phase Doppler Anemometry	√		‡	√
	Laser-Induced Incandescence	√		√	√
	Laser Diffraction		√	√	√
	Digital Holography		√		
Concentration	Light Extinction*	√			
	Mie Laser Scattering	√	√	√	√
	Phase Doppler Anemometry†	√			√
	Laser-Induced Incandescence	√		√	√
	Laser Diffraction		√	√	√
	Digital Holography		√		
Velocity	Laser Doppler Anemometry	√		‡	
	Phase Doppler Anemometry	√			√
	Digital Holography		√		

H: History, S: Snapshot, M: Model required, R: Refraction index of surrounding plasma required.
* Not simultaneously.
† Additional instrumentation/postprocessing required.
‡ Mie scattering model required for particles smaller than laser probe wavelength.

2.2.1 Light Extinction

This method uses the attenuation of the intensity of the light of a probe beam passing through plasma plume densely-laden with particles.[11] This is an *integral measurement technique*, meaning that it provides time resolved but spatially integrated—along the probe beam path—properties of the particulates/ plasma flow. This optical method is non-intrusive, as seen in Figure 8.

The intensity of a light beam going through a particulate laden plasma flow will be attenuated because scattering and attenuation by the particles. The temporal intensity changes of the probe light beam can be monitored using a photodetector. The Lambert-Beer law of light attenuation for a suspension of particles in a fluid is given by

$$\frac{I}{I_0} = \exp\left[-\frac{\pi}{4}\int_0^{D_{\max}}\int_0^{L} k(\lambda, D, n) D^2 N(D, x)\, dx\, dD\right], \tag{2}$$

where $k(\lambda, D, n)$ is the extinction coefficient—which can be estimated by the use of Mie elastic light scattering theory—, λ is the light wavelength, D is the particle diameter, n is the index of refraction of the gas/plasma surrounding the particulates, $N(D, x)$ is the particle number density distribution for particles sizes at point x along the probe light beam, and L is the probe beam path length through the plasma plume.

This equation shows that the light extinction depends on two particulates properties, particle diameter and particle number density concentration. Hence one of these properties must be foreknown to enable the measurement of the other parameter.

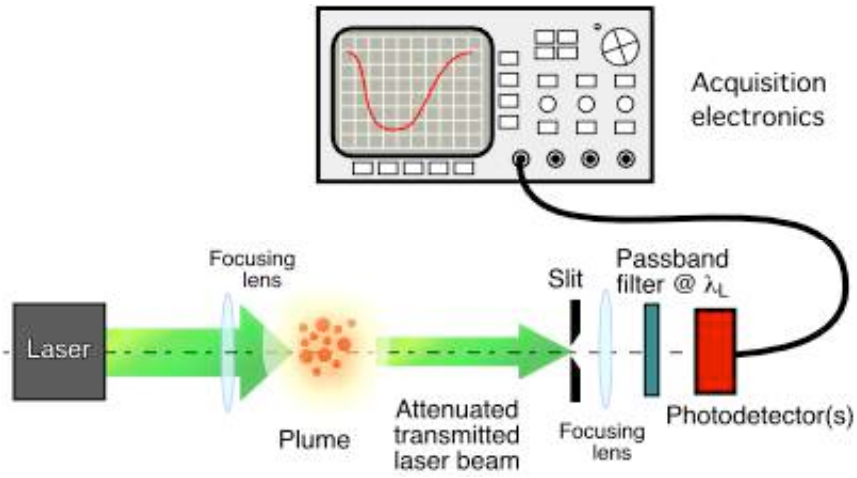

Figure 8- Optical layout for the Light Extinction method.

Although this method gives a fast response to the changes in particle concentration along the line of propagation of the probe beam, the requirement of the foreknowledge of the particle number density distribution along this line may lead to large measurement errors of all the relevant parameters. One of its advantages is that it does not require low particle concentrations immersed the gas/plasma flow.

2.2.2 Mie Elastic Light Scattering

The interaction of light beam with small particles results in the absorption and scattering of part of it. The angular dispersion pattern of the light scattered can be calculated using the theory of Mie[#] [12, 13, 14], which solves exactly the Maxwell's wave equations for the case of a plane electromagnetic wave scattering from homogeneous spheres immersed in a homogeneous refractive medium.

These solutions are—for unpolarized light—of the form

$$\frac{I}{I_0} = \frac{\left|S_1\left(\square, D, n_p / n_g, \square\right)\right|^2 + \left|S_2\left(\square, D, n_p / n_g, \square\right)\right|^2}{8\square k^2 r^2}, \tag{3}$$

Older treatments of the elastic light scattering by particles, subdivided the problem in three regions to simplify and approximate the complex and numerically intensive calculations. These regions are:

- ***Fraunhofer*** for $D < \square/10$;
- ***Mie*** or intermediate regime for $D \sim \square$.
- ***Geometrical optics***, for very large particles, i.e. $D > 4\square$.

The availability of cheap computational power, allowing the calculation using the full Mie elastic scattering equations, made this classification irrelevant.

where $S_1(\theta,D,n_p/n_g,\lambda)$ and $S_2(\theta,D,n_p/n_g,\lambda)$ are the Mie scattering phase (efficiency) functions for parallel and normal polarizations respectively, D is the particle diameter, θ is the angle of scattering with respect to the probe beam direction, n_p/n_g is the ratio of the indexes of refraction of particle and surrounding gas and k ($=2\pi/\lambda$) is the wavenumber of the probe laser light. Example plots of the phase functions $|S_1|^2$ and $|S_1|^2$ are shown in Figure 9, for several spherical particle sizes. These phase functions are complex infinite sums of spherical Bessel functions and Legendre polynomials. Full details on how to perform these calculations are in van de Hulst book [12].

Unfortunately, these phase functions are extremely sensible to variation on the particle size D. Three main angular regions of different behavior can be observed:

- In the narrow forward scattering range the scattered intensity is almost independent of the index of refraction of the particle, due to the dominance of diffraction effects. The scattered intensity varies as $\sim(D/\lambda)^4$.

- For off-axis locations and particle sizes below the probe laser wavelength λ, the phase function are proportional to $\sim(D/\lambda)^6$. For particles larger than the probe laser wavelength this proportionality changes to $\sim(D/\lambda)^2$. A plot of the phase function for unpolarized probe laser light forward scattered in aluminum is shown in Figure 10.

- Near the 90° scattering angle, the scattered intensity drops drastically compared with the other angles.

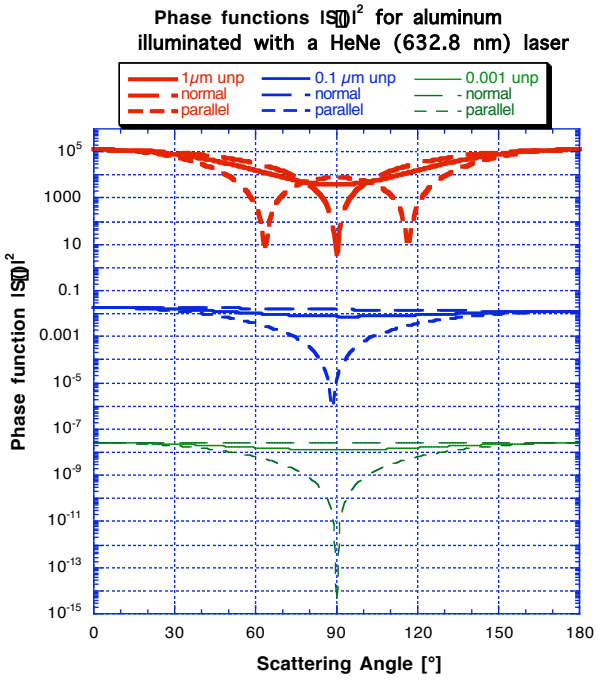

Figure 9- Angular pattern for the Phase Functions of HeNe (632.8 nm) laser light scattered by spherical Aluminum particles of diameters 10 nm to 1000nm.

To reduce the intensity fluctuations and to establish a smoother size intensity correlation, the aperture of the receiving optics may be increased so the scattered light can e collected from a wider angular region. Also white light can improve the smoothness of the response curve.

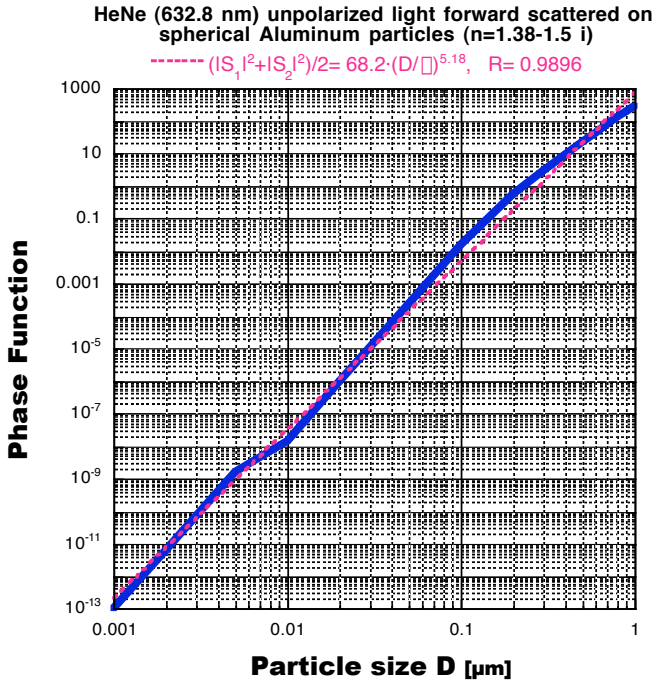

Figure 10- Phase function of forward scattered HeNe light for different Al spherical particle sizes.

2.2.2.1 Local Histories

In this configuration, a thin collimated laser beam passes through the plasma plume, being scattered by the particles immersed in it. The particulate concentration must be sparse, so there is only one scattering event per particle.

Surrounding the plasma plume there is an array of several optical fibers—tipped with focusing microlenses and optional polarizers—spaced uniformly angularly on the plane of a wide arc of circle, all pointing inwards to the center of symmetry of the plasma plume (see Figure 10). These fibers collect simultaneously the scattered light at different angles, and then relay it to an array of fast photodetectors or a linear CCD—all of them filtered with passband (in the probe laser wavelength) interference filters.

From the multiple measurements of scattered intensity obtained by the photodetector array, the angular patterns similar to those in Figure 9 can be fitted via non-linear calculations to find the particle size and distribution function parameters (some kind of foreknowledge of the functional form of the size distribution function would be always required) at a particular given time and position along the plasma plume expansion direction.

Using fast photodetectors with fast acquisition electronics, these multiple temporal traces of the scattered intensity allow obtaining a local history of the particle sizes passing through the sampled

region and the corresponding size distribution can be obtained for the duration of the plasma plume expansion.

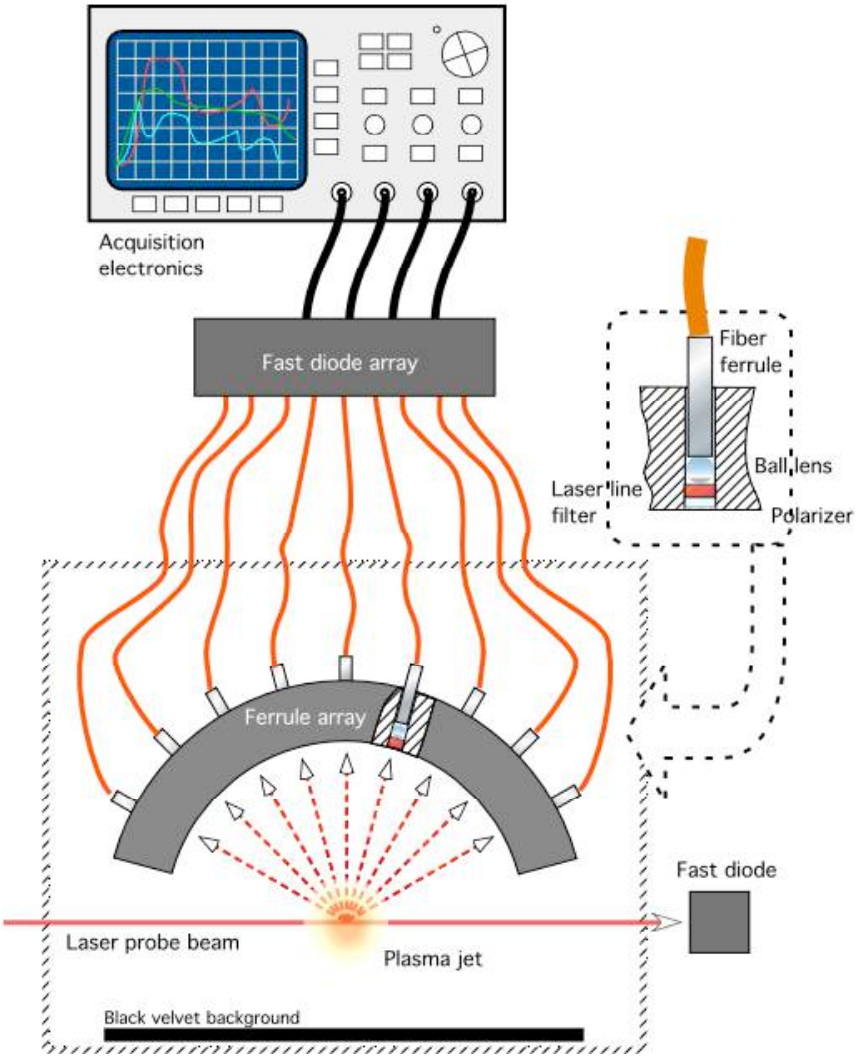

Figure 11- Optical layout for the Laser Light Scattering (Mie) method.

2.2.2.2 Full-plume snapshots

Unfortunately, getting a local history requires to take multiple measurements along the direction of expansion of the plasma plume to get the spatial evolution of the particulates immersed in it.

The previous optical setup can be modified to take a global snapshot of the scattered light by the entire particulate-laden plume at a single time. [15] A thin collimated laser sheet passes through the plasma plume, being scattered by the particles immersed in it. Again it is required that the particulate concentration to be sparse. Replacing the array of microlensed fibers by a single wide-angle cylindrical positive lens of large aperture —like a fish-eye— wider than the maximum expected plasma expansion distance, the elastically scattered light is collected and collimated (see Figure 13).

After collimation the beam can be compressed to fit into the CCD camera aperture size, and filtered with a narrow interference passband filter (at the probe laser sheet wavelength) to eliminate glare and optical noise from other sources.

As the angular intensity pattern of the scattered light is notoriously different for normal and parallel polarizations, a 50-50 beamsplitter cube can be positioned in front of the CCD camera to separate the S- and P- components before imaging.

The image of scattered light looks like those in Figure 12. From the angular signature of the CCD image lines, particle sizes and distributions can be calculated for each position along the plume expansion direction. Also information about particle formation, condensation and bunching, plus expansion velocity can be inferred from the examination of series of images taken consecutively.

Although this technique also suffers from the oversensitivity to scattering from larger particles, judicious use of field-of-view vignetting/masking and numerical image post-processing for contrast enhancement and mode filtering can potentially isolate and identify the contributions of smaller particles from the larges ones to the scattering pattern.

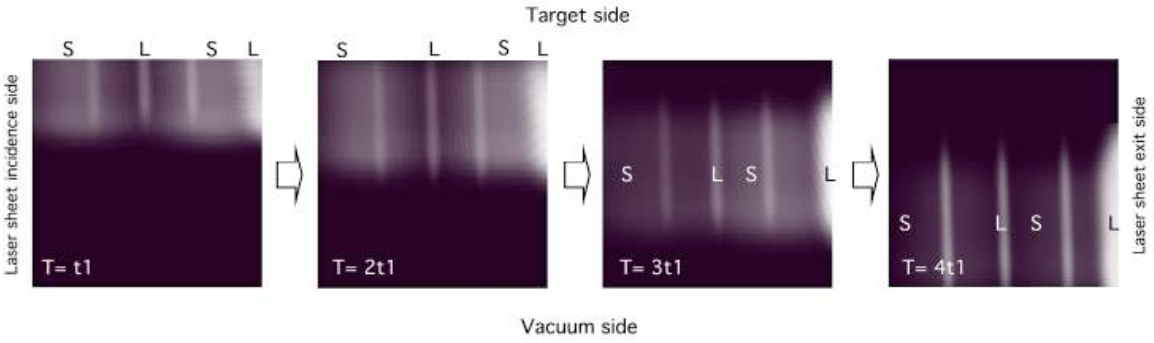

Figure 12- Time series of simulated images of a bimodal distribution of small and large particulates in a plume. S indicates the signature lobes for small particles, L the signature lobes for larger particles. In this case a mixture of large particles and small particles is ejected from te surface. The small particle light signature is to wide lobes, while the larger particles show a bright lobe near the forward scattering angles, plus several smaller narrow lobes elsewhere.

2.2.3 Doppler Anemometry

The availability of reliable and affordable laser light sources in the mid- to late Seventies, allowed the introduction of a family of instruments able to measure the particulates velocity—and in certain configurations size—by the interference of the light elastically scattered by the particles from pairs of coherent laser beams.

A succinct description of Laser- and Phase-Doppler Anemometry methods is presented in the next two sections. For the most comprehensive and modern single treatment on Doppler-related techniques, the reader is referred to the textbook by *Albrecht etal* [16].

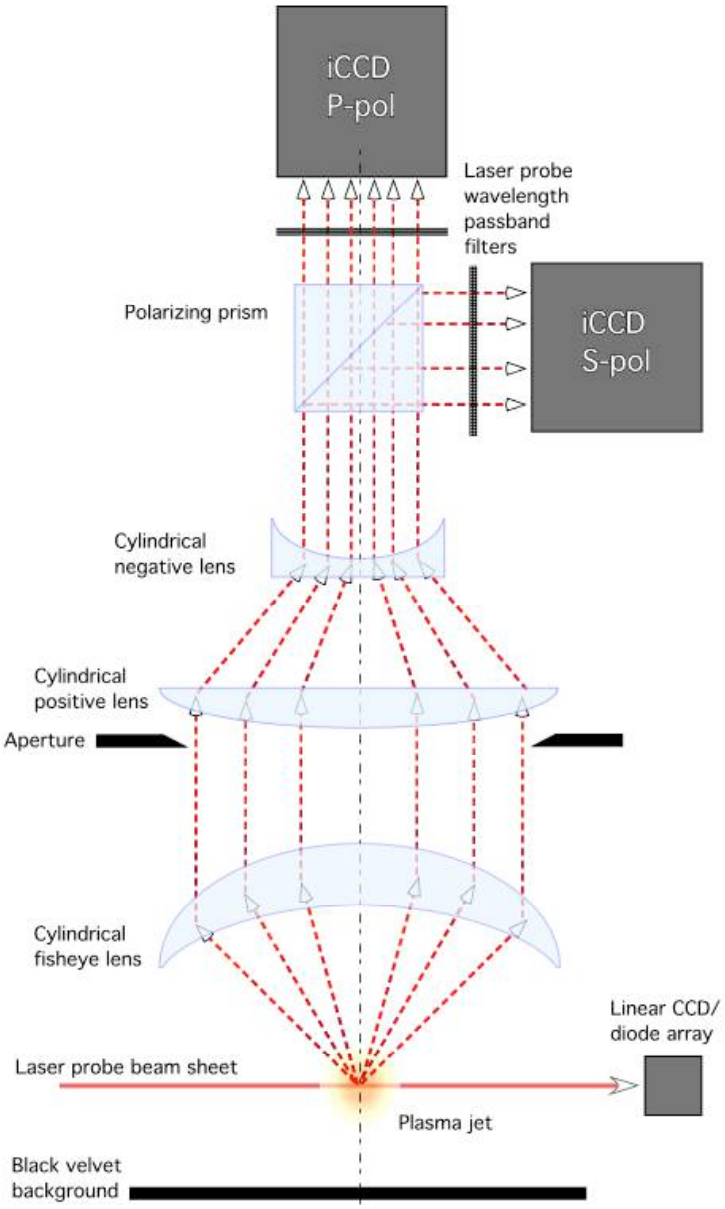

Figure 13- Diffractive Imaging Laser Light scattering (Mie) method.

2.2.3.1 Laser-Doppler—LDA

The laser-Doppler technique samples the flow velocity at discrete times corresponding to the passage of a particle through the intersection volume of two thin laser probe beams. As submicron-sized particles immersed in the plasma plume pass through the intersection of two laser beams, the scattered light received from the particles fluctuates temporally in intensity.

The frequency of this fluctuation is equivalent to the Doppler shift between the incident and scattered light, and is thus proportional to the component of particle velocity which lies in the plane of the two laser beams and is perpendicular to their bisector. The velocity direction can be fixed if

one of the laser beams has a frequency slightly different from that of the other, resulting in a positive or negative constant frequency offset of the measured signal.

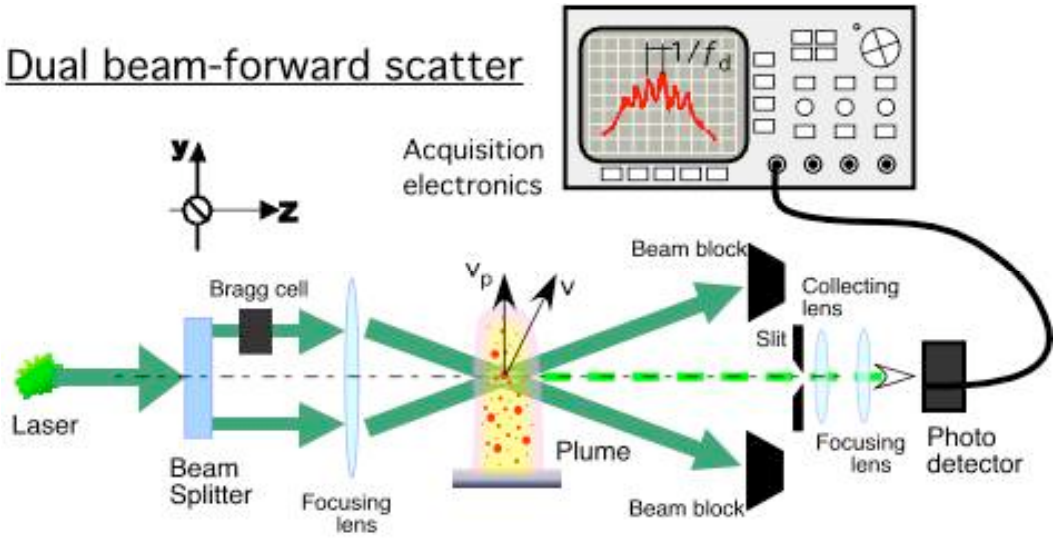

Figure 14- Optical layout for Laser-Doppler Anemometry.

Crossing 4 or 6 laser beams of different wavelengths or polarization in the same measuring volume, and separating out the scattered light using filters can measure all 3 components of velocity. The frequency is measured using digital counters (if data rates are above 50 per second) or photon correlators (low data rates and signal level) or spectral analyzers (Doppler shift frequency not over a few Megahertz). For particulate sizes smaller than the laser probe beams wavelength l the optical signal at the detector—for a dual-beam forward scatter instrument—is

$$I(t) = I_0\left[1+\cos\left(2\pi\frac{v_p t}{\lambda}\sin\frac{\theta}{2}\right)\right]. \qquad (4)$$

The normal component of the velocity in the plane of intersection of the laser beams then is given by

$$v_p = \frac{\lambda}{2\sin(\theta/2)} f, \qquad (5)$$

where f is the frequency of oscillation of the detected signal.

This method gives spatially precise point measurements (0.5% for wind-tunnel systems!) of the particle velocity, at speeds from mm/s up to highly supersonic.

A laser power source is required, with excellent frequency stability, narrow line width, small beam diameter, and a Gaussian beam intensity profile (bright at the center). Typically, HeNe or Argon ion lasers are used, with power levels from 10 mW to 20 W.

This method has several limitations, such as

- *Single-point measurement.*
- *Data arrival times dictated by particle arrival in the measuring volume, not when user wants to sample data.*
- *Particle velocity and its derivatives will differ substantially from flow velocity in vortex cores and across shocks.*
- *Small particles could not produce signals above the noise threshold.*
- *Greater noise at higher speeds (radio frequency interference possible).*
- *Signal level depends on detector solid angle, posing problems of optical access.*
- *Mie scattering intensity is much better in the forward direction, but it is difficult to set up forward receiving optics, which remain aligned to the moving measurement volume.*
- *Optics alignment time ranges from 3 hours for a 1-component system to a day for a 3-component system: may be sensitive to vibrations. These problems may be alleviated with fiber optic probes, at the cost of signal level due to fiber power loss.*

2.2.3.2 Phase-Doppler—PDA

The Laser-Doppler technique does not provide information on the size or structure of the particles sampled within the measurement volume defined by the intersecting probe beams. To do so time delays or phase difference among the particle-scattered signals, therefore requiring the use of two or more photodetectors, emplaced at different angular positions.

The Phase-Doppler Anemometry (also known as Particle Dynamics Analysis) is an online optical technique that allows the simultaneous measurement of the velocity and size of spherical particles. Similarly to the Laser-Doppler Anemometry, of which this method is an extension, PDA is a local measurement technique that looks at single particles in a small sampling volume, defined by the intersection of two thin probe laser beams.

A spherical particle will act as a mirror and/or a lens that will make the parallel rays of the incident probe beams to fan-out in different directions after partial reflection and/or refraction, as seen in Figure 16. Therefore, the scattered light is not uniform in intensity for all directions, depending also in the values of the particle and surrounding gas indexes of refraction. The position of the photodetectors must be carefully selected so only one mode of light scattering is dominant. For totally reflecting or strongly absorbent particles, the forward scattering range is not to be used, because diffraction effects destroy the linearity of the phase-size relation.

The particle velocity is the same as in equation (4), but now the particle size can be obtained from the phase difference Δ between the signals from the two photodetectors. This phase difference Δ is given by

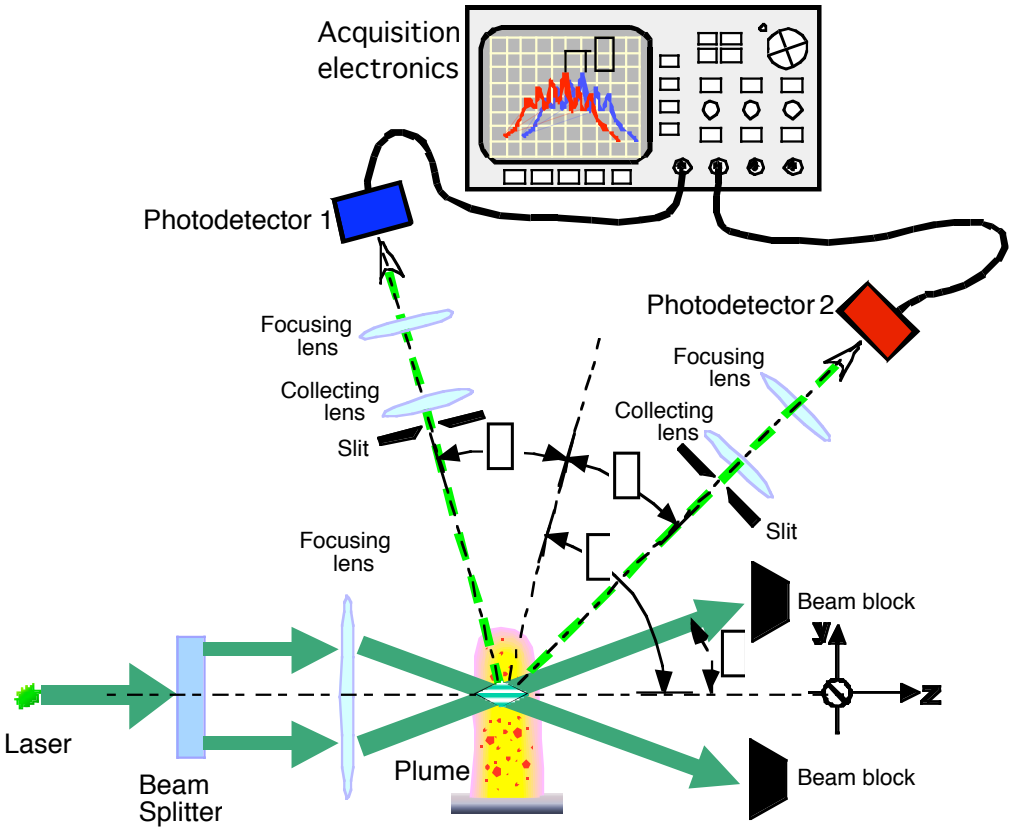

Figure 15- Optical layout for Phase-Doppler Anemometry.

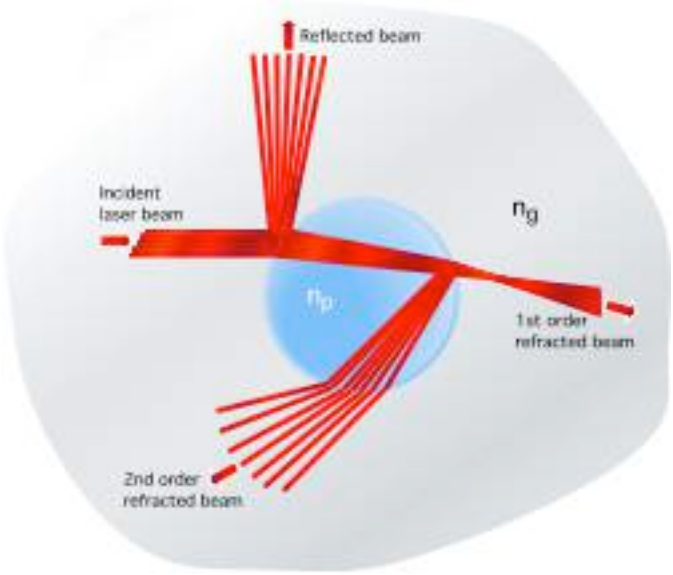

Figure 16- Reflection and refraction of a collimated beam by a spherical particle immersed in a gas/plasma.

$$\Phi = \begin{cases} 2\pi\dfrac{D}{\lambda}\dfrac{\sin\theta\sin\phi}{\sqrt{2(1-\cos\theta\cos\phi\cos\beta)}} & \text{, for reflection.} \\ 2\pi\dfrac{D}{\lambda}\dfrac{\frac{n_p}{n_g}\sin\theta\sin\phi}{\sqrt{2(1+\cos\theta\cos\phi\cos\beta)\left[1+\frac{n_p^2}{n_g^2}-\frac{n_p}{n_g}\sqrt{2(1+\cos\theta\cos\phi\cos\beta)}\right]}} & \text{, for refraction.} \end{cases} \quad (6)$$

where the angles θ, ϕ, β are defined as in Figure 15- Optical layout for Phase-Doppler Anemometry.; n_p and n_g are the indexes of refraction of the particle and surrounding gas.

This equations is obtained using geometrical optics, therefore the particle size must be larger than the wavelength of the laser light probe beams, so no interference from Mie elastic scattering modes is considered. [12] The theoretical analysis of LDA systems has and can be extended to include these scattering effects (including beam polarization), as for small particles diffraction represents an especially important contribution to the total signal and can disturb the phase measurement. [13]

The maximum particle size that can be unambiguously measured with two photodetectors corresponds to a phase Φ =360°. Reducing the angle β between detectors can extend the particle size range, at the cost of reducing resolution. Adding a third detector at a small angle β allows both to have a large size range and resolution (see Figure 17). Use of linear CCD arrays can improve the spatial and temporal resolution by increasing the size of the statistical sampling for a single measurement [17].

As an extension of the Laser-Doppler technique Phase-Doppler Anemometry shares its practical and economical advantages and limitations as seen in the previous section, although has the benefit of providing accurate measurements of particle size, and through the use of fast time-series and correlation instrumentation, even concentration measurements can be done with confidence.

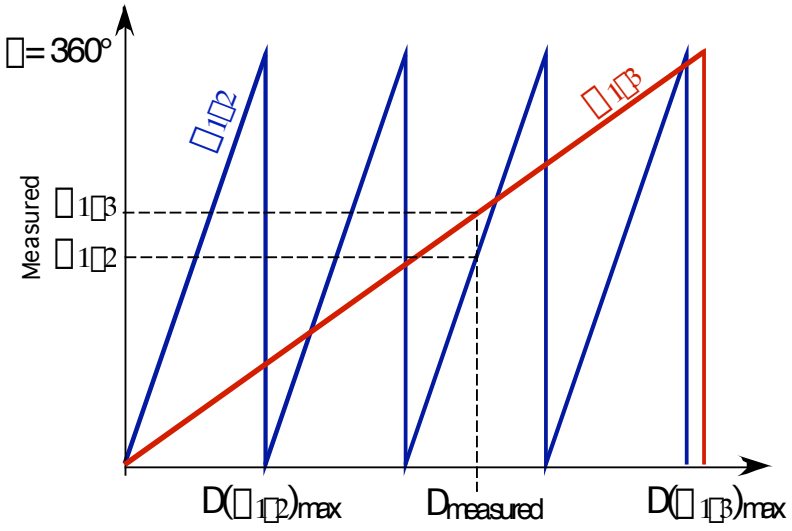

Figure 17- Phase size relations for a three-detector Phase-Doppler system.

2.2.4 Photon Correlation Spectroscopy

In photon correlation spectroscopy (PCS) or quasi-elastic light scattering (QELS) the Brownian motion (movement in random direction) of sub-micron particles is measured as a function of time. [18]

A laser beam is diffracted by particles in suspension. The diffusion of particles causes rapid fluctuations in scattering intensity around a mean value at a certain angle (varying from 10 to 90°). These intensity fluctuations depend on particle size. The calculated correlation function results in a diffusion coefficient for a given temperature and viscosity which can be converted to particle size.

2.2.5 Laser-Induced Incandescence

Laser-induced incandescence (LII) occurs when an intense laser beam encounters particulate ejecta. A particle can absorb energy from the beam, which causes the particle's temperature to increase. At the same time, the particle can loose energy by heat transfer mechanisms to the surroundings. If the energy absorption rate is sufficiently high, the temperature will rise to levels where significant incandescence (essentially blackbody emission) and vaporization can occur. As larger particles shed their thermal energy slower than the smaller ones, LII can be used to obtain information about the size distribution of all the ejected particles within a measurement volume.

For particles much smaller than the wavelength of the scattered light (i.e. in the Rayleigh scattering regime) the efficiency of scattering decreases drastically as the scattered intensity is proportional to the sixth power of the particle radius. Therefore other kinds of laser interaction with the particles can provide more sensitive detection techniques. In this context Laser Induced Incandescence (LII) method is a valuable tool for the characterization of nanoparticles.

LII has become a standard method for in-situ particle size detection, allowing one to determine particle size and density from a single measurement. Melton[19] first proposed it as a technique for soot concentration measurement. Consequently, LII has been used in various applications and used as a diagnostic tool in combustion flames, diesel engines and exhaust flows.[20,21] A detailed review of LII approach is given by Santoro etal.[22] More recently, LII has successfully been applied in the detection of carbon nanotubes[23] and metal nanoparticles.[24,25]

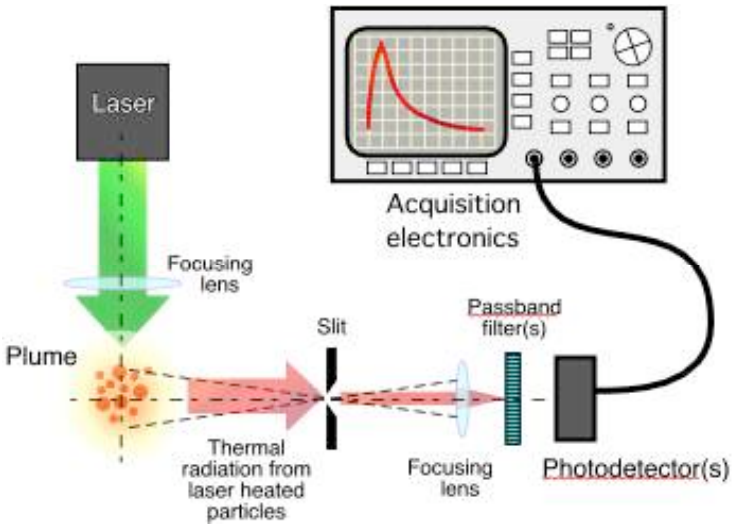

Figure 18- Optical layout of the Laser-Induced Incandescence method.

The method is based on the heating of the particles by a short laser pulse and the subsequent detection of the thermal radiation emitted by the particles. In a typical LII experiment, a pulsed laser is used to heat up the particles. The particles are heated to a temperature well above the surrounding gas temperature due to absorption of laser energy. The heated particles start to emit thermal radiation as they cool. The cooling can be via three possible ways: vaporization, heat conduction and radiation. The LII signal decay reflects the cooling process of the particles caused by evaporation and heat conduction.

The incandescence signal is collected and the particle size is determined by the detection of the temporal decay of the LII signal using a fast photodetector. The LII signal decay is numerically simulated using a LII model. The parameters describing the particle size is varied until the calculated decay of the LII signal is in accordance with the measured one. The temporal evolution of the LII signal gives the particle size while the height of the signal is proportional to the particle density.

The LII model is based on energy and mass balance between the particle and the surrounding gas. The intensity of LII signal depends on a number of factors. The dominant factor is the temperature of the laser-heated particles, which in turn depends on the rate of laser energy absorption and heat loss through conduction, radiation and particle vaporization. Fundamentally the generation of LII signal is complicated by dependencies on particle size, particle temperature, surrounding gas temperature, laser energy intensity, laser beam profile and other parameters such as the detection wavelength.

The incandescence signal in time is given by[26]

$$S_{LII}(t) = \alpha D(t)^2 \frac{\Omega}{4\pi} \int_0^{\infty} G_{\lambda}(\lambda) Q_{\lambda,par}\left[D(t)\right] e_{\lambda,bb}\left[T_{par}(t)\right] d\lambda \qquad (7)$$

where D is the particle diameter, T_{par} is the particle temperature, Ω is the optics collection solid angle, G_{λ} is the combined spectral response function of the photodetector(s) and its optics, $Q_{\lambda,par}$ is the spectral emissivity, $e_{\lambda,bb}$ is the black body spectral emissive power.

The LII method may be applicable in determining the small size particles in laser-produced plasmas. The main concern will be extracting the LII signal from the background plasma emission. The selection of the spectral region at which to detect the LII signal can be quite wide. Time gated detection may be useful in LII signal extraction.

The Laser-Induced Incandescence method has several limitations [27]

- *High ejecta concentration/long optical path lengths can lead to attenuation of laser across the plasma plume flow field or attenuation of incandescence between measurement volume and detector*
- *Requires high intensity laser (>50-100 MW/cm2) for Nd:YAG lasers*
- *Requires detector with short temporal gating capability (<50 ns for lasers with 5-10 ns pulse durations)*
- *The detection wavelength must be chosen to minimize broadband fluorescence interference from the plasma/gas background.*

2.2.6 Laser diffraction

In laser diffraction (static light scattering) [28] the circular scattering pattern, obtained from illumination of dispersed particles with a laser beam, contains information about the particle size. The interaction between particles and light is mainly dependent on particle size, shape, surface roughness and the refractive indices of material and the dispersing medium. For particles larger than the laser probe wavelength most of the light is scattered in the forward direction as a result of diffraction.

For a specific material, the circular scattering pattern of a particle is unique for its size, and given by the Airy function

$$I(D,r) = cI_0 \frac{\pi^2 D^4}{16 f^2} 2 \frac{J_1\left(\frac{\pi Dr}{\lambda f}\right)}{\frac{\pi Dr}{\lambda f}}, \qquad (8)$$

where J_1 is the first-order spherical Bessel function, f is the transform lens focal length and r is the radius from the center of the detector (see Figure 19- Optical arrangement for particle sizing by laser diffraction.). Deconvolution of the sample scattering circular pattern with an optical model such as Mie results in the particle size distribution.

The technique is especially applicable to samples with a broad or bimodal distribution and for information on size trends in series of samples. It is used extensively to analyze particle samples and two-phase flows.[29, 30, 31]

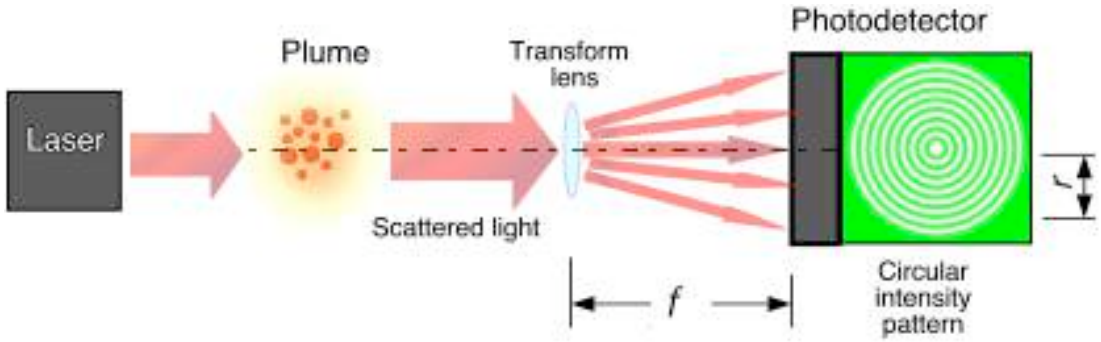

Figure 19- Optical arrangement for particle sizing by laser diffraction.

2.2.7 Cavity Ringdown Laser Spectroscopy

The Cavity Ringdown Laser Spectroscopy (CRLS) developed by O'Keefe [32] has been extensively reviewed [33, 34, 35]. It is very sensitive and suitable for aerosol detection. CRLS has recently been introduced as a method to determine the aerosol extinction coefficient [36, 37, 38]. It makes use of an resonant optical cavity formed by two highly reflecting mirrors. When a short light pulse from a tunable laser is injected into the cavity through the input mirror, the laser pulse is reflected back and forth inside the cavity. The light intensity decays due to losses in the cavity and

the exponential decay is characterized by the cavity ringdown time t_c. The intensity of the emerging light is described by

$$I(t) = I_0 \exp\left(-\frac{t}{t_c}\right) \qquad (9)$$

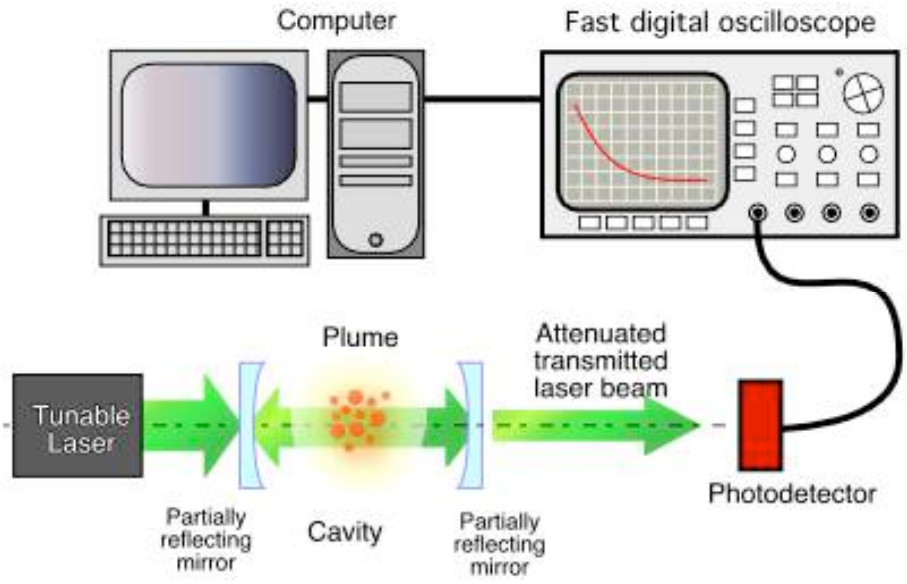

Figure 20- Schematic of a cavity ringdown spectrometer.

If an absorbing species is introduced into the cavity, its presence will increase the losses. As a result the cavity ringdown time will be shorter than that observed with a cavity that does not contain the absorbing species. The light emerging from the output mirror is detected by a photomultiplier tube. The ringdown signal produced by the photomultiplier then will be analyzed and processed using a Digital Oscilloscope and a computer where the data points would be fitted to an exponential decay curve with a characteristic time constant.

In the presence of an absorbing species, the extinction coefficient α_e is given by

$$\alpha_e = \frac{1}{c}\left(\frac{1}{t_c} - \frac{1}{t_0}\right), \qquad (10)$$

where t_0, t_c are the characteristic time in the cavity with just dry air and absorbing medium respectively.

The aerosol particles, when illuminated by a laser beam, scatter and absorb some of the light. The ratio of the transmitted light to the incident light is given by

$$I(t) = I_0 \exp(-\alpha_e L) \qquad (11)$$

where L is the path length of the laser beam through the aerosol. The particle extinction coefficient is related to the particle extinction efficiency by [39]

$$\beta_e = NAQ_E, \qquad (12)$$

where $A = \pi d^2/4$ for homogeneous monodisperse spherical particles and N is the number concentration of the particles.

For polydisperse particles, eqn. (10) holds good for each particle size s, and the combined extinction coefficient [39] will be

$$\beta_e = \sum_S \frac{\pi}{4} N_S D_S^2 Q_{e,s} \qquad (13)$$

For very small particles and for big particles, Q_e is readily calculated. For particles less than 50 nm in diameter [39], Q_e is given by

$$Q_e = \frac{8}{3}\left(\frac{\pi d}{\lambda}\right)^4 \left(\frac{m^2 - 1}{m^2 + 2}\right) \qquad (14)$$

For large particles (> 4 microns) Q_e approaches 2, its limiting value. For particles between 50 nm and 4 microns, Q_e can be calculated using computer calculations [40].

An interesting characteristic of Q_e is its dependency upon the size parameter, $\alpha = \pi d/\lambda$.

The characterization of the size parameter requires independent information on the diameter of aerosols. The experimentally determined values of Q_e are plotted against the size parameter α and then compared with the corresponding theoretical Q_e function determined using computer calculations [40].

2.2.8 Digital Holographic particle sizing

The fundamental idea in this technique is to consider the diffracted field with particles and record that diffracted field as a hologram. This hologram is reconstructed to form an image of the original three-dimensional sample.

With holography the whole 3-Dimensional particle distribution can be recorded. The use of high resolution CCDs and fast computers makes the recording of the holograms and the reconstruction of the object wave feasible. This technique, called Digital Holography, is real holography where the object and reference wavefronts are recorded on a CCD camera producing an intensity pattern from which diffracted wavefronts can be reconstructed numerically.

A simple schematic of the digital holographic set up is given in Figure 21. A laser sheet passes through the particulate-laden plasma plume and the hologram is recorded directly by a CCD. The hologram is reconstructed and the particle size distribution and velocity is calculated numerically.

The minimum particle size that can be determined with the holographic technique depends on the laser wavelength used for recording the hologram. Digital holographic technique using pulsed lasers offers recording of transient events (speed limited by the laser pulse duration) of small particles and can be reconstructed later. The technique has been applied to the study of laser induced optical breakdown event on solid targets. [40]

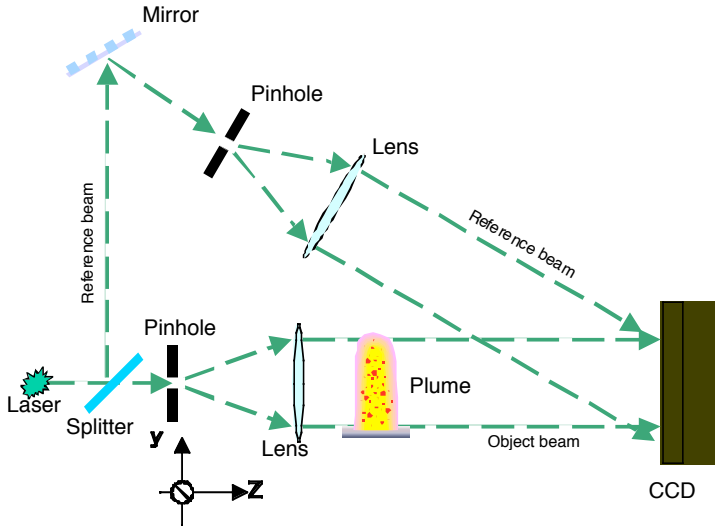

Figure 21- Optical layout for Particle Sizing using Digital Holography.

This method, although allows an easy qualitative 3D geometrical analysis from the reconstructed image, also requires the implementation of extremely complex wavefront reconstruction computer algorithms for CCD recording and quantitative analysis.

3. CONCLUSIONS

Laser based diagnostic techniques have been surveyed for in situ time resolved measurement of particle size, velocity, number density of aerosol particles in IFE relevant ablation plumes. Laser based techniques have become increasingly popular and important in particle sizing. Use of lasers allow detailed real time measurements to be made in hostile environments not accessible by other types of particle sizing methods.

It is useful to divide the techniques into two general categories based on whether a technique analyze single particle or aggregate of particles. Single particle counters generally determine size of a single particle at a time. At high concentrations, single particle techniques suffer from errors when more than one particle occupies the same region at the same moment. The second class of techniques, called ensemble techniques generally make measurements on large number of particles. They measure the average size distribution of a group of particles. They are suited for measurements at high particle concentration but become less effective at low concentration of particles.

The choice of a particular diagnostic technique must be done considering the particle properties that need to be measured and the conditions under which the measurement has to be done. There is no single technique capable of fully characterizing aerosols. Only through a combination of two or more techniques can aerosols be diagnosed completely. Of the optical techniques described, the combined use of methods such as Cavity ringdown laser spectroscopy, Dark Field imaging, Laser Induced incandescence offer the best hope for effective characterization of aerosols in transient laser ablation plumes. These are compatible techniques with the potential of characterizing size, velocity and composition of aerosol particles.

APPENDIXES

A- Other optical methods

A.1 Schlieren imaging

A Schlieren instrument records changes in the refractive index distribution of transparent media like gaseous/plasma flows. The refractive index distribution can then be related to density, temperature, or pressure distributions within the flow.

A white light source is usually used to minimize diffraction fringes. The source is passed through a thin slit, and then collimated by either a mirror or a lens. The collimated light is passed through the flow and then brought to a focus.

The focal spot is an image of the source slit if the flow is uniform; it is aberrated by the flow otherwise. A knife-edge placed at the focus is positioned so that it blocks roughly half of the light. If the flow is uniform, then the image behind the knife-edge will be uniformly bright.

If the flow has refractive index variations that cause some of the light that would have passed by the knife-edge to instead be blocked by it, then the image has dark areas. Conversely, if the flow causes some light rays to pass the knife-edge that would otherwise have been blocked, then the image has brighter areas (see Figure 22).

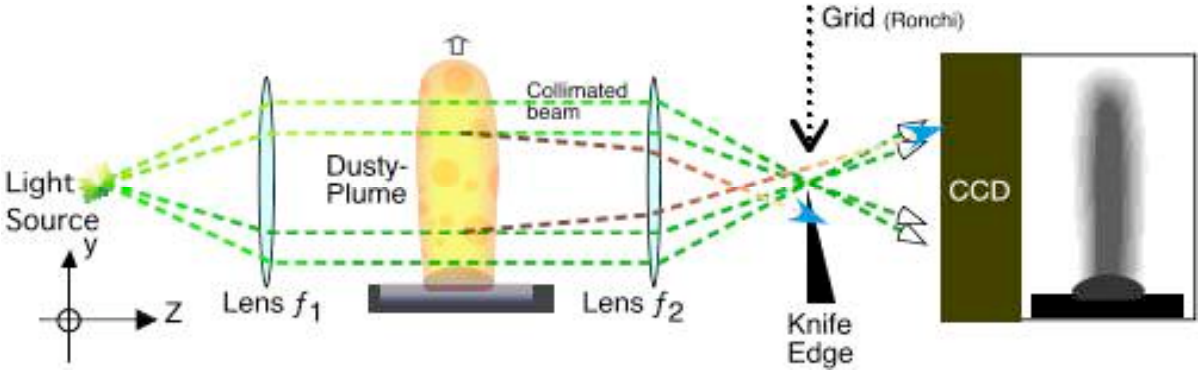

Figure 22- Optical layout for Schlieren Imaging.

A.2 Velocity Interferometry—VISAR

This technique is commonly used to obtain precise (1-2%) velocity histories of the motion at the interface of a shock-loaded material with a light transmitting media. Called Velocity Interferometer System for Any Reflector—VISAR [41]—, it uses a laser light beam, which is reflected from the (usually mirrored) surface of a shocked specimen. This beam is then split; one part beam delayed several nanoseconds, and then recombined with the undelayed portion of the beam. The undelayed part has a frequency equal to that of the laser plus the Doppler shift imparted by the moving surface; the delayed portions has the laser frequency plus the Doppler shift existing a short (delay) time τ

earlier. Figure 23 shows a schematic of the optical layout for a VISAR in its Wide Angle Michelson Interferometer (WAMI) configuration.

It can be shown [42, 43] that the velocity u of the moving surface is

$$u(t) = \frac{\lambda}{2} = \frac{\lambda F(t)}{2\left(1 + \frac{\Delta\lambda}{\lambda_0}\right)}, \qquad (15)$$

where λ is the laser wavelength, t is the time, $F(t)$ is the interferometer fringe count number (zero for a stationary surface) and $\Delta\lambda/\lambda_0$ is a correction factor depending in the index of refraction of the transparent media at the specimen interface—equal to zero for air/vacuum.

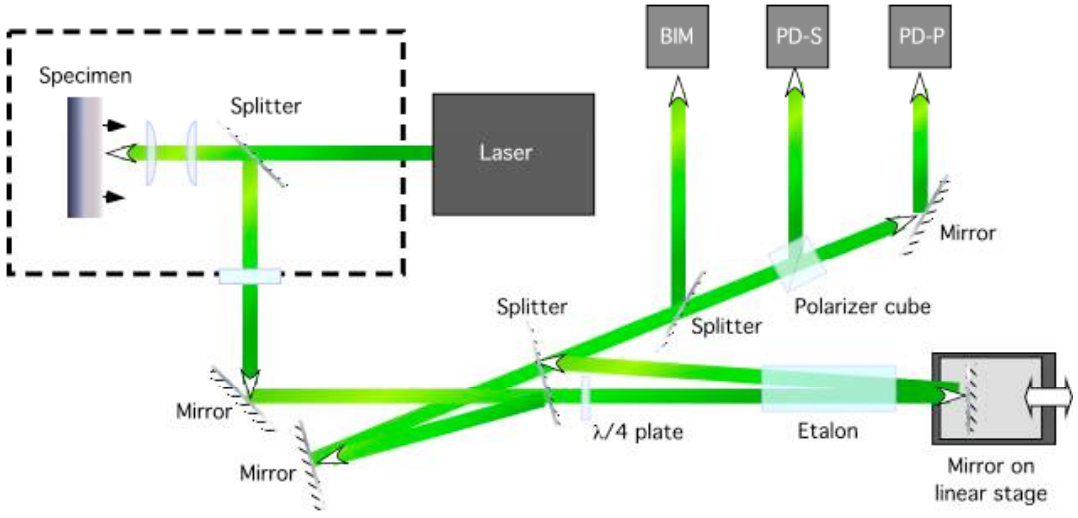

Figure 23- Optical layout for a VISAR-WAMI.BIM is the Beam Intensity Monitor, PD-S and PD-P are the photodetectors for S- and P-polarization respectively. Counting how many circuits the point given by the signal amplitudes of PD-S and PD-P traces around a circle of radius determined by the signal amplitude of the BIM, *F(t)* can be calculated at anytime.

A.3 Dark-Field Imaging/Scattering of the laser-heated target surface.

This method was developed originally to detect flaws or dust contamination on high quality optical surfaces. [44,.45, 46]

Similar to the technique describes in section 2.1.3, the collimated probe laser light is reflected from the target surface or scattered by any particle or irregularity on/near the surface. The reflected collimated light is collected and focused by a condenser lens—which is focused on the reflecting surface—into a beam block; the scattered component is also collected and collimated through an imaging lens into a probe laser wavelength filtered CCD.

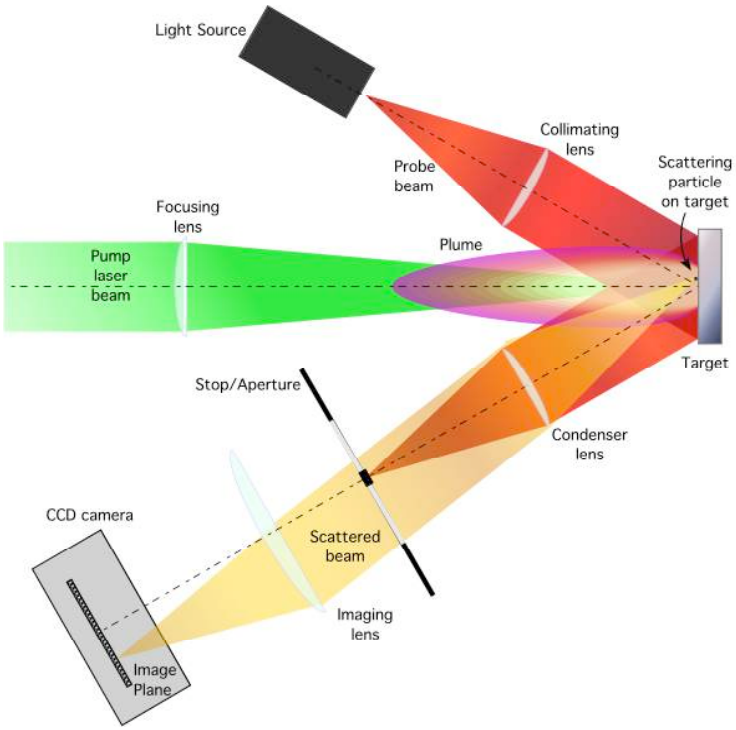

Figure 24- Optical layout for Dark Field Imaging of the laser-heated target surface.

B- Spherical particle penetration distance in a gas.

A spherical particle moving in a gas will experience an aerodynamic drag force that will stop its motion after a certain distance X_p. Assuming that the motion of the sphere is at a Reynolds number small enough that the Stokes [47] formula for the drag can be applied, then the one-dimensional equation of motion for the spherical particle is

$$\frac{4}{3}\pi\left(\frac{D^3}{8}\right)\rho\frac{d^2x}{dt^2} = -6\pi\mu\left(\frac{D}{2}\right)\frac{dx}{dt} \qquad (16)$$

D is the particle diameter and ρ is its mass density, μ (=1.81 g/cm·s for dry air at STM conditions) is the surrounding gas viscosity and x is the traversed distance at time t. Then the solution to this equation is

$$x(t) = \frac{\rho D^2 u_0}{18\mu}\left[1-\exp\left(-18\frac{\mu}{\rho D^2}t\right)\right] \qquad (17)$$

where u_0 is the initial particle speed before entering the gas. Therefore the maximum penetration distance for the spherical particle will be

$$X_p = \frac{\rho D^2 u_0}{18\mu} \qquad (18)$$

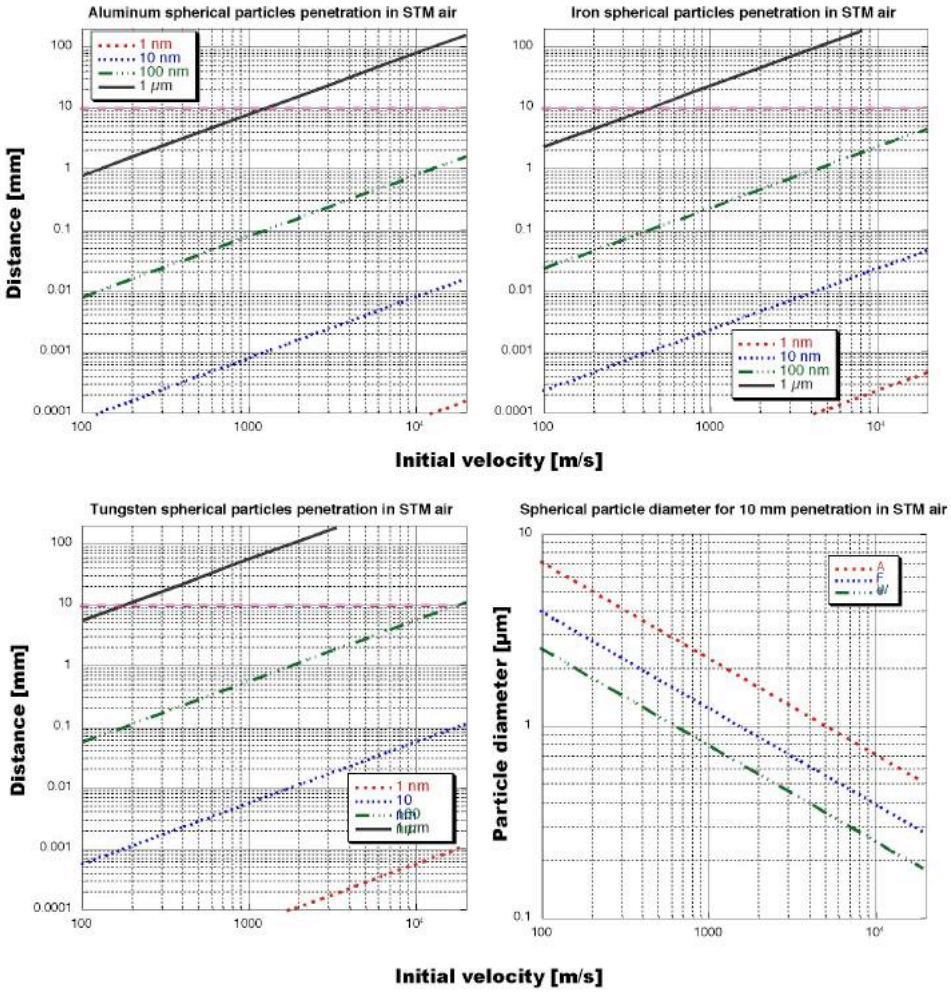

Figure 25- Penetration distance for a spherical particle in STM air.

Figure 25 shows three plots (two at top, lower left) of the penetration distance for spherical particles of aluminum (ρ = 2.7 g/cm^3), iron (ρ = 7.9 g/cm^3), and tungsten (ρ = 19.2 g/cm^3) in dry air at standard atmospheric conditions (1 atm, 25°C). The lower right plot shows the required particle diameter to penetrate 10 mm of standard dry air, again for aluminum, iron and tungsten.

C- Particle Distribution functions

Some distribution functions [48] for particulates in common use are

C.1 Log-normal

$$f(D) = \frac{1}{\sqrt{2\pi}\sigma_0 D}\exp\left[-\frac{\ln(D/D_M)}{2\sigma_0}\right]. \qquad (18)$$

C.2 Rosin-Rammler

$$f(D) = \frac{k}{D}\left[\left(\frac{1}{k}+1\right)\frac{D}{D_M}\right]^{k-1}\exp\left[-\left(\frac{1}{k}+1\right)\frac{D}{D_M}\right]^{k}. \qquad (19)$$

Γ is the gamma function.

C.3 Log-hyperbolic

$$f(D) = \frac{\sqrt{\alpha^2 - \beta^2}}{2\alpha K_1\left[\delta\sqrt{\alpha^2-\beta^2}\right]}\exp\left\{-\alpha\sqrt{\delta^2+\left(\ln\frac{D}{D_M}\right)^2}+\beta\ln\frac{D}{D_M}\right\}. \qquad (20)$$

K_1 is the Bessel function of the third kind.

D- Index of Refraction Formulas for gases and plasmas

The index of refraction of a neutral gas is given by the well-known Lorentz-Lorenz [49] equation

$$\frac{n^2-1}{n^2+2} = \frac{4}{3}\pi N\alpha \qquad (21)$$

where N is the number density of molecules of polarizability α. The product $N\alpha$ is usually of order 10^{-4} at one atmosphere and 0°C.

For the index of refraction of a magnetized plasma, the Appleton-Hartree equation [50] is used; with

$$n^2 = 1 - \frac{X(1-X)}{1-X-\frac{1}{2}Y^2\sin^2\theta \pm Y\sqrt{\frac{1}{4}Y^2\sin^4\theta+(1-X)^2\cos^2\theta}} = 1 - \Phi(X,Y,\theta), \qquad (22)$$

where $X=\omega_{pe}^2/\omega^2$, $Y=\omega_B/\omega$, and θ is the angle between the local magnetic field and the direction of propagation of the light beam. $\omega_B = eB/m_e$ is the plasma cyclotron frequency, $\omega_{pe} = 4\pi n_e e^2/m_e$ is the plasma electron frequency, and ω the light frequency.

For a gas/plasma mixture the total index of refraction follows the modified Lorentz-Lorenz equation

$$\frac{n^2-1}{n^2+2} = \frac{4}{3}\pi\left[\sum_{species} N_s\alpha_s - \frac{\Phi(X,Y,\theta)}{3-\Phi(X,Y,\theta)}\right] = \sum_{species}\frac{N_s}{N_{s0}}\frac{n_{s0}^2-1}{n_{s0}^2+2} - \frac{1}{4\pi}\frac{\Phi(X,Y,\theta)}{1-\Phi(X,Y,\theta)/3} \qquad (23)$$

with N_s is the number density of molecules of species s with polarizability α_s., while all the same species parameters with subindex 0 are taken at 1 atm. and 0°C. When the index of refraction n is very close to 1, then we get the approximated value

$$n \approx 1 + \sum_{species}\frac{N_s}{N_{s0}}(n_s-1) - \frac{\Phi(X,Y,\theta)}{3-\Phi(X,Y,\theta)}. \qquad (24)$$

Literature overview:

Several reviews are available on the topic of in situ measurement of particles. David Black et al have reviewed the significance of laser based particle sizing techniques in 1996 [52]. *Aerosol Measurement: Principles, Techniques and Applications* edited by Paul Baron and Klaus Willeke [53] is an excellent book that provides detailed discussions on aerosol fundamentals and measurement techniques. Another source of information is the July 2000 issue of Journal of aerosol scicence and technology and the 1991 November Issue of Applied Optics.

Some texts provide detailed discussions of particle size distribution types, optical properties of aerosols and the theory of particle measurement techniques. These include Aerosol Technology by Hinds [54], Particle size measurement by Allen [55], and Modern methods of Particle size analysis by Barth [56].

REFERENCES

1 B.Christensen and M.S.Tillack, '*Survey of mechanisms for liquid droplet ejection from surfaces exposed to rapid pulsed heating*,' UCSD-ENG-100, January 2003.

2 Examples of commercially available instruments for aerosol and particulates measurement can be found in the WWW corporate pages for TSI at http://www.tsi.com, and for Horiba at http://www.horibalab.com.

3 P.Bowen, '*Particle Size Distribution Measurement from Millimeters to Nanometers and from Rods to Platelets'*, J. of Dispersion Sci. and Tech **23**, 631 (2002).

4 D.Blair and M.S.Tillack, '*The effect of ionization on cluster formation in laser ablationplumes'*, UCSD-ENG-XXX, August 2003.

5 H.0.Barth, and R.B.Flippen, '*Particle Size Analysis*' Anal. Chem. **67**, 257R (1995).

6 S.H.Jeong, O.V.Borisov, J.H.Yoo, X.L.Mao, and R.E.Russo, '*Effects of Particle Size Distribution on Inductively Coupled Plasma Mass Spectrometry Signal Intensity during Laser Ablation of Glass Samples'*, Anal.Chem. 71, 5123 (1999).

7 R.R.Whitlock and G.M.Frick, '*Particle size distributions of aerosols formed by laser ablation of solids at 760 Torr'*, J. Mater. Res. **9**, 2868 (1994).

8 D.T. Suess, K. A. Prather, Chem Rev., **99**, 3007 (1999).

9 G.Videen, M.G.Turner, V.J.Iafelice, W.S.Bickel, and W.L.Wolfe, '*Scattering from a small sphere near a surface*', J.Opt.Soc.Am **A 10**, 118 (1993).

10 G.Videen, '*Ligh scattering from a sphere behind a surface*', J.Opt.Soc.Am **A 10**, 110 (1993).

11 C.Crowe, M.Sommerfeld, and Y. Tsuji, *'Multiphase Flows with Droplets and Particles'*, Chapter 9, pp.303-304, CRC Press (1997).

12 H.C.Van de Hulst, *'Light Scattering by Small Particles'*, Dover (1981).

13 DANTEC/Invent, *'STREU, A computational code for the light scattering modes of spherical particles'*, Instruction manual, 1994

14 A.R.Jones, '*Light scattering for particle characterization'*, Progress in Energy and Combustion Science **25**, 1 (1999).

15 Y-L.Pan, K.B.Aptowicz, R.K.Chang, M.Hart, and J.D.Eversole, '*Characterizing and monitoring respiratory aerosols by light scattering*', Opt. Lett. **28**, 589 (2003).

16 H.-E.Albrecht, M.Borys, N.Damaschke, and C.Tropea, '*Laser Doppler and Phase Doppler Measurement Techniques'*, Springer (2002).
Also see the WWW pages of DANTEC at http://www.dantecdynamics.com/ for very colorful and detailed descriptions of commercial LDA and PDA systems.

17 J.Rheims, T.Wriedt, and K.Bauckhage, '*Working Principle and Experimental Results for a Differential Phase-Doppler Technique*', Part. Part. Syst. Charact. **15**, 219 (1998).

18 R.Pecora, '*Dynamic light scattering measurement of nanometer particles in liquids'*, J. of Nanoparticle Res. **2**, 123 (2000).

19 L.A.Melton, Appl. Opt. **23,** 2201 (1984).

20 R.L.Vander Wal and K.J.Weiland, '*Laser-induced incandescence: development and characterization towards a measurement of soot volume fraction'*, Appl Phys B **59,** 445 (1994).

21 P.O.Witze, S.Hochgreb, D.Kayes, H.A.Michelson and C.R.Shaddix, '*Time-Resolved Laser-Induced Incandescence and Laser Elastic-Scattering Measurements in a Propane Diffusion Flame'*, Appl. Opt. **40**, 2443 (2001)

22 R.J.Santoro and C.R.Shaddixls, in '*Applied Combustion Diagnostics,'* K.Kohse-Hoeinghaus and J.B Jeffries (ed.) Taylor & Francis, p.252 (2002).

23 R.L.Vander Wal, G.M.Berger, T.M.Ticich and P.D.Patel, '*Application of Laser-Induced Incandescence to the Detection of Carbon Nanotubes and Carbon Nanofibers'*, Appl. Opt. **41,** 5678 (2002).

24 R.L.Vander Wal, T.M.Ticich and J.R.West, '*Laser-induced Incandescence Applied to Metal Nanostructures'*, Appl. Opt. **38,** 5867 (1999).

25 A.V.Filippov, M.W.Markus and P.Roth, '*In-situ characterization of ultrafine particles by laser-induced incandescence: sizing and particle structure determination'*, J. Aerosol Science **30**, 71 (1999).

26 B.Mewes and J.M.Seitzman, '*Soot volume fraction and particle size measurements with laser-induced incandescence*', Appl. Opt. **36,** 709 (1997).

27 R.L. Vander Wal, '*Laser-induced incandescence: detection issues'*, Appl. Opt. **35,** 6548 (1996).

28 C.Crowe, M.Sommerfeld, and Y. Tsuji, *'Multiphase Flows with Droplets and Particles'*, Chapter 9, pp.304-308, CRC Press (1997).

29 Z.Ma, H.G.Merkus, J.G.A.E.de Smet, C.Heffels, and B.Scarlett , '*New developments in particle characterization by laser diffraction: size and shape*', Powder Technology **111**, 66 (2000).

30 J.Swithenbank, J.U.Beer, D.S.Taylor, D.Abbot, and G.C.McCreath, '*A laser diagnostic technique for the measurement of droplet and particle distribution'*, Prog. in Astro. and Aero., AIAA 421 (1977)

31 D.E.Hirleman, V.Oechsle, and N.A. Chigier, '*Response characteristics of laser diffraction particle size analyzers: Optical sample volume extent and lens effects*', Optical Engineering, **23**, 610 (1984).

32 A.O'Keefe, D.A.G. Deacon, Rev.Sci.Instru. **59,** 2544 (1988).

33 K.W.Busch and M.A.Busch, *'Cavity Ringdown Spectroscopy'* ACS Symp Series (1999).

34 G.Berden, R.Peeters and G.Meijer, Int. Rev. Phys.Chem. **19,** 565 (2000) and references therein.

35 J.J.Scherer, J. B. Paul, A.O'Keefe and R.J.Saykally, Chem.Rev. **97,** 25 (1997) and references therein.

36 A.D.Sappey. E.S.Hill, T.Settersten and M.A. Linne, Opt.Letts. **23,** 954 (1998).

37 J.D.Smith and D.B.Atkinson, The Analyst **126,** 1216 (2001).

38 V.Bulatov, M.Fisher, I.Schechter, Anal. Chimi. Acta **466,** 1 (2002).

39 W.C.Hinds, *'Aerosol Technology'* John Wiley & Sons (1982).

40 Z.Liu, G.J.Steckman, and D.Psaltis, '*Holographic recording of fast phenomena'*, Appl. Phys. Letts **80,** 731 (2002).

41 L.M.Barker, and R.E.Hollenbach, '*Laser interferometer for measuring high velocities from any reflecting surfaces'*, J. Appl. Phys **43**, 4669 (1972).

42 L.M.Barker, and R.E.Hollenbach, '*Shock Wave Studies of PMMA, Fused Silica, and Sapphire'*, J. Appl. Phys, **41**, 4208 (1970).

43 D.R. Goosman, '*Analysis of the laser velocity interferometer'*, J. Appl. Phys **46**, 3516 (1975).

44 D.C.Weber and E.D.Hirleman, '*Light Scattering signatures of individual spheres on optically smooth conducting surfaces'*, Appl. Opt. **27,** 4019 (1988).

45 P.A.Robbert, and J.Vlieger, '*Light scattering from a sphere on a substrate'*, Physica **137A**, 209 (1986).

46 J.H. Kim,S.H.Ehrman, G.W.Mulholland, and T.A.Germer, '*Polarized light scattering by dielectric and metallic spheres on silicon wafers'*, Appl. Opt. (2002).

47 G.K.Batchelor, '*An Introduction to Fluid Dynamics'*, p.233 Cambridge Univ. Press (2000).

48 C.Crowe, M.Sommerfeld, and Y. Tsuji, *'Multiphase Flows with Droplets and Particles'*, Chapter 3, CRC Press (1997).

49 L.A.Vasil'ev, '*Schlieren methods'*, chapter IX, Israel Prorgam for Scientific Translations (1971).

50 I.H.Hutchinson, *'Principles of Plasma Diagnostics'*, pp. 91-93, Cambridge Univ. Press (1987).

52 D. L. Black, M.Q. McQuay and M.P. Bonin*, Laser Based Techniques for particle size measurment: A review of sizing methods and their industrial applications*, Prog. Energy.Combust.Sci **22** pp.267-306. (1996)

53 P A Baron and K Willeke, *Aerosol measurement: Principles, Techniques and Applications*, Wiley Interscience (2001)

54 W. C. Hinds, Aerosol Technology: Properties, Behavior and Measurement of airbone particles, Wiley Interscience (1982)

55 T. Allen, Particle size measurement, Chapman and Hall (1981)

56 H.G.Barth, Modern methods of particle analysis, Wiley Intescience (1984)